J. Mt. Sci. (2020) 17(9): 2108-2122 e-mail: jms@imde.ac.cn http://jms.imde.ac.cn
https://doi.org/10.1007/s11629-019-5772-5

Evaluation of spatiotemporal variability of temperature and precipitation over the Karakoram Highway region during the cold season by a Regional Climate Model

YANG Tao[1,2,3,4,5,6] https://orcid.org/0000-0002-7382-2983; e-mail: yangtao515@mails.ucas.ac.cn

LI Qian[1,2,3,7] https://orcid.org/0000-0002-1555-4167; e-mail: liqian0109@mails.ucas.ac.cn

CHEN Xi[1,3,5,7] https://orcid.org/0000-0003-0432-0733; e-mail: chenxi@ms.xjb.ac.cn

YIN Gang[8] https://orcid.org/0000-0002-8941-0078; e-mail: chinayg@xju.edu.cn

LI Lan-hai[1,2,3,7*] https://orcid.org/0000-0003-4573-6284; e-mail: lilh@ms.xjb.ac.cn

Philippe De MAEYER[1,4,5,6] https://orcid.org/0000-0001-8902-3855; e-mail: philippe.demaeyer@ugent.be

** Corresponding author*

1 State Key Laboratory of Desert and Oasis Ecology, Xinjiang Institute of Ecology and Geography, Chinese Academy of Sciences, Urumqi 830011, China

2 Ili Station for Watershed Ecosystem Research, Chinese Academy of Sciences, Xinyuan 835800, China

3 University of Chinese Academy of Sciences, Beijing 100049, China

4 Department of Geography, Ghent University, Ghent 9000, Belgium

5 Sino-Belgian Joint Laboratory of Geo-information, Urumqi 830011, China

6 Sino-Belgian Joint Laboratory of Geo-information, Ghent 9000, Belgium

7 Research Centre for Ecology and Environment of Central Asia, Chinese Academy of Sciences, Urumqi 830011, China

8 College of Resources and Environmental Sciences, Xinjiang University, Urumqi 830046, China

Citation: Yang T, Li Q, Chen X, et al. (2020) Evaluation of spatiotemporal variability of temperature and precipitation over the Karakoram Highway region during the cold season by a Regional Climate Model. Journal of Mountain Science 17(9). https://doi.org/10.1007/s11629-019-5772-5

Abstract: Precipitation and temperature are two important factors associated to snow hazards which block the transport infrastructure and cause loss of life and properties in the cold season. The in-situ observations are limited in the alpine with complex topographic characteristics, while coarse satellite rainfall estimates, reanalysis rain datasets, and gridded in-situ rain gauge datasets obscure the understanding of the precipitation patterns in hazard-prone areas. Considering the Karakoram Highway (KKH) region as a study area, a double nested Weather Research and Forecasting (WRF) model with the high resolution of a 10-km horizontal grid was performed to investigate the spatial and temporal patterns of temperature and precipitation covering the Karakoram Highway region during the cold season. The results of WRF were compared with the in-situ observations and Multi-Source Weighted-Ensemble Precipitation (MSWEP) datasets. The results demonstrated that the WRF model well reproduced the observed monthly temperature (R = 0.96, mean bias = -3.92°C) and precipitation (R = 0.57, mean bias = 8.69 mm). The WRF model delineated the essential features of precipitation variability and extremes, although it overestimated

Received: 05-Sep-2019
Revised: 26-May-2020
Accepted: 17-Jul-2020

the wet day frequency and underestimated the precipitation intensity. Two rain bands were exhibited in a northwest-to-southeast direction over the study area. High wet day frequency was found in January, February, and March in the section between Hunza and Khunjerab. In addition, the areas with extreme values are mainly located in the Dasu-Islamabad section in February, March, and April. The WRF model has the potential to compensate for the spatial and temporal gaps of the observational networks and to provide more accurate predictions on the meteorological variables for avoiding common cold-weather hazards in the ungauged and high altitude areas at a regional scale.

Keywords: Karakoram Highway; WRF model; Precipitation; Temperature; Snow hazards

Introduction

Precipitation is one of the most important elements in hydrology, meteorology and the ecosystem in mountainous areas. The dominant regional climate systems of the Karakoram are the westerlies during December to March and the Indian Summer Monsoon from June to September (Cannon et al. 2015). The precipitation that westerlies brought accounts for more than 50% of the annual precipitation in the Karakoram during winter time (Lang and Barros 2004). The precipitation during the cold season is generated from the westerlies and could maintain the glaciers, e.g. the glaciers in the upper Indus River basin (Anders et al. 2006; Tahir et al. 2011; Ridley et al. 2013; Boltch et al. 2012; Cannon et al. 2015). In addition, heavy orographic precipitation often occurred in the Karakoram's high mountains due to the interaction between these climate systems and topography (Cannon et al. 2017). Extreme precipitation events cause risks of hazards including floods, snow avalanches, debris flows, and mountain torrents, leaving the transport infrastructure in this regions highly exposed to hazards (Koks et al. 2019). These snow related hazards block the transport infrastructure, mainly the Karakoram Highway (KKH) during the cold season, especially in spring (Kreutzmann 2004). Previous studies showed that the westerlies' activity would increase in the 21st century, generating more winter precipitation and further complicating the regional dynamics of the climatic systems (Ridley et al. 2013). Extreme events such as hot extremes and heavy precipitation may become more frequent and intense in this region, leading to more risks such as severe floods and other hazards (Houze et al. 2011). Thus, it is important to reveal the precipitation patterns during the cold season for water management and hazard protection.

The in-situ observations for climatic parameters are limited in the complex topographic areas in the Karakoram and Himalaya, especially in the high elevation. Satellite rainfall estimates, reanalysis rain datasets, and gridded in-situ rain gauge datasets can be supplemented for in-situ measurements. For instance, the datasets from the Global Precipitation Climatology Centre (GPCC) (Schneider et al. 2014), Climatic Research Unit (CRU) (Harris et al. 2014), and the Asian precipitation highly resolved observational data integration towards evaluation (APHRODITE) (Yatagai et al. 2012) are based on the interpolation of in-situ rain gauges. The satellite and gauge combined rainfall datasets, including the tropical rainfall measurement mission (TRMM) (Huffman et al. 2007) and Climate Hazards Group InfraRed Precipitation with Station data (CHIRPS) (Funk et al. 2015). However, each dataset has its deficiencies. The satellite precipitation estimates, such as TRMM, have a large deviation in the cold season (Rasmussen et al. 2012; Lettenmaier et al. 2015), as well as suffer from the short records. Furthermore, the gauge-only gridded datasets have disadvantages in low spatial resolution (usually ≥ 0.5°), relative low temporal resolution (CRU, monthly data), and uncertainties in the ungauged areas after interpolation. In addition, the coarse spatial resolution in the reanalysis datasets also obstructs the regional climate research. Thus, the precipitation products, which are merged from the gauge, satellite, and reanalysis data, have been developed (Sun et al. 2018). The accuracy of the merged precipitation products is higher than the individual product's (Xie and Xiong 2011). The Multi-Source Weighted-Ensemble Precipitation (MSWEP) is a merged precipitation product with a high temporal (3-hour) and spatial resolution (0.1°) on a global scale with long period (Beck et al. 2017, 2019). It reported a high accuracy compared with 22 precipitation products using rain gauges and hydrological modeling at global scale (Beck et al.

2020), and has been successfully applied for studying water resources from global to regional scales (Chen et al. 2017; Chen and Dirmeyer 2017; Schellekens et al. 2017; Yang et al. 2020). However, uncertainties still exist due to data-less ground-validation regarding the complex terrains and high elevation areas.

It is important to know the annual total precipitation because it directly influences the hydrological processes, while the frequency and intensity in daily precipitation is linked to the natural hazards and the health of the ecosystem. However, it is difficult to reveal the precipitation patterns at high elevations due to the limited observations. A regional climate model (RCM) could enable the capture of the climatological characteristics, as well as its finer spatial resolution in the general circulation models (GCMs). Furthermore, the RCM dynamically downscales the high-resolution projections of climate change scenarios for the future (Gula and Richard Peltier 2012; Tang et al. 2016; El-Samra et al. 2017). The Weather Research and Forecasting (WRF) model employed as a RCM is a useful approach for regions with complex topographies that can not be resolved by coarse GCMs (Antic et al. 2006; Skamarock et al. 2005; Skamarock and Klemp 2008). A number of studies demonstrated that the WRF could reveal the climate characteristics in Asia (Qiu et al. 2017; Karki et al. 2018), North America (Liu et al. 2017; Wang et al. 2018), Europe (Argüeso et al. 2012; Cardoso et al. 2013; Erlandsen et al. 2017; Avolio and Federico, 2018) and China (Maussion et al. 2011; Yuan et al. 2012; Li et al. 2018; Liu et al. 2019). For the extreme precipitation, although there exists a bias in the exact location and intensity with the observations, the WRF model could well reproduce the essential features of the extreme precipitation events in the mountainous area (Ikeda et al. 2010; Fernández-González et al. 2015; Norris et al. 2015; Karki et al. 2018). These studies showed implications on water resources management, and provided adaptation strategies and measures for potential risks on a regional scale.

Aiming to reveal the patterns in temperature and precipitation over Karakoram and the Himalaya area, many studies employed the WRF model to dynamically downscale the interannual variability and seasonality of the meteorological variables in this region. Norris et al. (2019) found contrasting trends regarding the precipitation and temperature from 1979 to 2015, which is associated with different trends in the glaciers of the central Himalaya and the Karakoram region. Maussion et al. (2014) demonstrated the patterns of precipitation on monthly to annual scales by the WRF model and generated an 11-year period dataset, called the High Asia Reanalysis (HAR). Gao et al. (2015) analyzed the variations in temperature and precipitation of 32 years in the Tibetan Plateau by the WRF downscaling method. However, these studies mainly focused on the basic features of precipitation in the entire High Mountain Asia and Tibetan Plateau, and insufficiently documented the extreme precipitation.

In this study, concerning the relevant natural hazards caused by a single factor or coupling factors of precipitation and temperature during the cold season, the WRF model was performed over the Karakoram Highway region from October to April during the period 2010 to 2015. The results were compared with the in-situ observations and MSWEP precipitation datasets. The main objectives addressed by this study include: (1) to investigate the capacity of the WRF model in reproducing the spatiotemporal distribution of temperature and precipitation during the cold season in the region where the in-situ observations are scarce, and (2) to highlight the areas with high frequency and intensity of precipitation during the cold season over the KKH. The results could provide a reliable prediction on the meteorological variables related to snow hazards and information for the water resources' management in the ungauged and high altitude areas by the WRF model at regional scale.

1 Methodology

1.1 Study area and model domains

The Karakoram Highway, linking the southern coast of Pakistan to the inland part of Central Asia, constitutes the life line for the regional economic needs of northern Pakistan. The road goes from the Khunjerab Pass (4500 m asl) to the plain area in Pakistan (below 1000 m). The study area holds a

diverse and complex landscape ranging from deep canyons (Hunza Valley, Gilgit Valley) and snow-covered high peaks (Rakaposhi, 7788 m) with heights from < 1000 m to > 8000 m asl (Ashraf et al. 2012). The upper Indus River basin is located within the study area, which provides the important fresh water resources for the country. The study area also comprises many glaciers, making it as one of the world's most glaciated areas (Hasson et al. 2014). The regions are influenced by mid-latitude westerlies during winter, receiving winter precipitation from the Mediterranean Sea from December to March (Dimri et al. 2015; Asmat and Athar 2017). The summer precipitation occurs as a result of the monsoon originating from the Bay of Bengal from July to September (Dimri et al. 2015; Asmat and Athar 2017). The Gilgit and Hunza Valleys are two of the driest areas of Central Asia (Ashraf et al. 2012). The appreciable winter precipitation (snowfall) and < 0°C temperature occur at high elevations in winter and cause associated snow hazards along the KKH (Derbyshire et al. 2001). Figure 1 shows the sketch map, indicating the model simulation area and meteorological stations in the study area.

1.2 Model setup and validation

The model was run on one-way double-nested domains with a horizontal grid at 30 km (d01) and 10 km (d02), respectively (as shown in Figure 1a). The inner domain d02 covers the area from Khunjerab to Islamabad. The coarse domain d01 had 61 × 62 grid points in the west-east and south-north direction and the second domain d02 was nested with 61 × 61 grid points. The vertical structures counted 30 levels in all domains with the top located at 50 hPa. The initial and lateral boundary conditions for three domains were used from the NCEP Global Final Analyses (FNL) data available at 1 × 1 degree 6-hourly (http://dss.ucar.edu/datasets/ds083.2/) and the sea surface temperature was obtained from the ERA-Interim dataset. The simulation began from 00:00 UTC of September 1, 2010 and ended at 18:00 UTC of April 30, 2015 at 6-h intervals. The first month was used for the spin-up. The parameterization schemes followed and were adjustified by previous studies (Norris et al. 2015, 2017) and were presented in Table 1, including the Kain-Fritsch Cumulus Scheme (Kain 2004), the Rapid Radiation Transfer Model (RRTM) for the longwave radiation (Mlawer et al. 1997), the Dudhia shortwave radiation model (Dudhia 1989), the WRF Single-Moment 3-Class microphysics model, the Noah Land Surface Model (Noah LSM) (Chen and Dudhia 2001) and the Yonsei University model for the planetary boundary layer (YSU) (Hong and Lim 2006). In order to evaluate the performance of the WRF model, the monthly temperature and precipitation from the WRF model were compared with monthly in-situ observations, and the extreme precipitation was evaluated by MSWEP dataset.

1.3 Data

There are 17 meteorological stations in the study area (Figure 1b). Three stations at daily scale

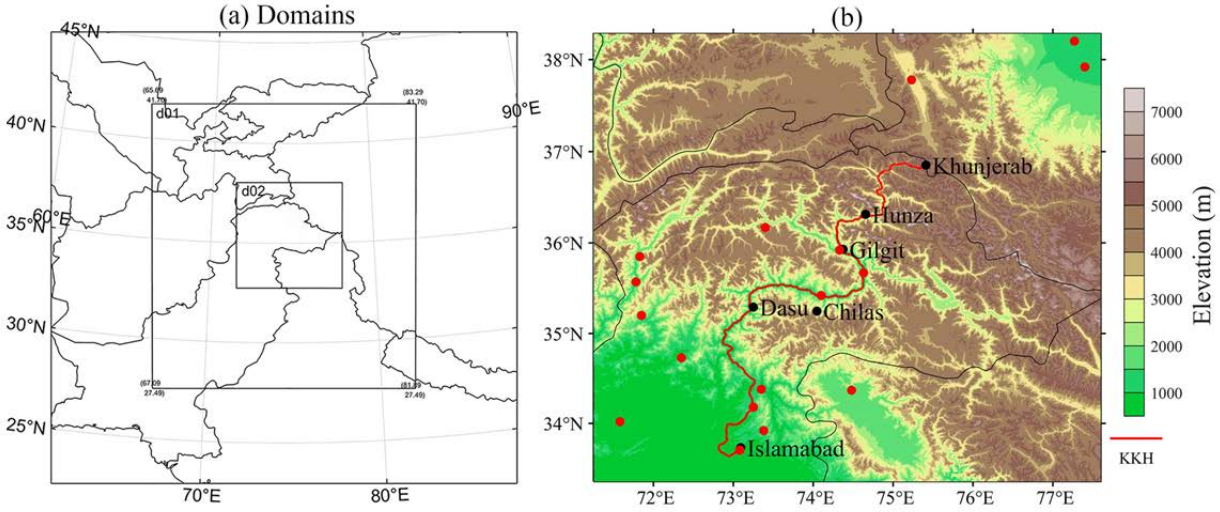

Figure 1 Model simulation area (a) and the topography of study area (b). Red dots, black dots, and red line represent the meteorological stations, the cities, and Karakoram Highway (KKH), respectively.

were collected from the Chinese meteorological dataset version 3.0 (http://data.cma.cn/site/index.html). Fourteen stations at monthly scale were obtained from the National Climatic Data Centre (https://www.ncdc.noaa.gov/wdcmet). These data were strictly processed and quality controlled before release (See Table 2). The monthly precipitation value from the in-situ observations was used to evaluate the simulated results from the WRF model.

The Multi-Source Weighted-Ensemble Precipitation (MSWEP) V2.2 is a global precipitation dataset covering 1979 to 2017 with a 3-hour temporal resolution and a 0.1°× 0.1° spatial resolution (Beck et al. 2019). It was generated by merging the satellite and reanalysis precipitation data by weighed averaging, and correcting by gauge precipitation. This merging method enabled its reliability with higher accuracy than individual precipitation estimates (Beck et al. 2020). Several studies have confirmed the high performance of MSWEP dataset in main land China, India, and Pakistan where our study area covered (Prakash 2019; Ullah et al. 2019; Xu et al. 2019). This dataset was employed to compare the extreme precipitation of the simulated results from the WRF model on a daily scale.

1.4 Evaluation method

The output from the WRF model was assessed by the in-situ observations. The temperature and precipitation values from the nearest grid cells of the WRF model were compared with the in-situ observations on a mean monthly basis. The mean bias (MB), Root Mean Square Error (RMSE), and correlation coefficient (R) were used to evaluate the performance of the WRF model, and they could be calculated using:

$$MB = \frac{1}{N}\sum_{t=1}^{N}\left(Sim_{(t)} - Obs_{(t)}\right) \quad (1)$$

$$RMSE = \sqrt{\frac{1}{N}\sum_{t=1}^{N}\left(Sim_{(t)} - Obs_{(t)}\right)^2} \quad (2)$$

$$R = \frac{\sum_{t=1}^{N}\left[\left(Sim_{(t)} - Sim_{mean}\right)\left(Obs_{(t)} - Obs_{mean}\right)\right]}{\sqrt{\sum_{t-1}^{N}\left(Sim_{(t)} - Sim_{mean}\right)^2 \sum_{t-1}^{N}\left(Obs_{(t)} - Obs_{mean}\right)^2}} \quad (3)$$

where N is the total observed or simulated number, t is the time step, Sim(t) and $Obs(t)$ are the observed and simulated values at time t, respectively, and Sim_{mean} and Obs_{mean} are the mean of the observed and simulated values, respectively.

Table 1 Main physical parameterizations used in the numerical simulations

Simulation period	2010-2015
Nest	2
Horizional grid (innermost)	10 km
Number of grids (innermost)	61×61
Vertical Levels	30
Microphysics' scheme	WSM-3
Longwave radiation scheme	RRTM
Shortwave radiation scheme	Dudhia
Planetary boundary layer	YSU
Cumulus parameterization	Kain-Fritsch
Initial/lateral boundary condition	FNL
Land surface model	Noah

Notes: WSM-3: Single-Moment 3-Class microphysics model. RRTM: Rapid Radiation Transfer Model. YSU: Yonsei University model. FNL: NCEP Global Final Analyses data.

Table 2 The information of meteorological stations used for the Weather Research and Forecasting model validation.

Station number	Name	Lat. (N)	Long. (E)	Alt. (m)	Period
41506	Chitral	35.85°	71.83°	1499	2011-2012
41508	Dir	35.20°	71.85°	1369	2011-2012
41515	Drosh	35.57°	71.78°	1464	2011-2015
41523	Saidu Sharif	34.73°	72.35°	961	2011-2012
41530	Peshawar	34.02°	71.58°	359	2011-2015
41535	Kakul	34.18°	73.25°	1308	2011-2012
41536	Balakot	34.38°	73.35°	980	2011-2012
41573	Murree	33.92°	73.23°	2167	2011-2012
41577	Islamabad	33.70°	73.38°	543	2011-2012
43504	Gupis	36.17°	73.40°	2155	2011-2012
43516	Gilgit	35.92°	74.33°	1459	2011-2012
43518	Bunji	35.67°	74.63°	1372	2011-2012
43519	Chilas	35.42°	74.10°	1250	2011-2012
43532	Muzaffarabad	34.37°	73.48°	701	2011-2012
51804	Taxkorgan	37.78°	75.23°	3094	2010-2015
51814	Yarkand	37.92°	77.40°	1360	2010-2015
51815	Zepu	38.20°	77.27°	1275	2010-2015

2 Results and Discussion

2.1 Spatial and temporal patterns of the monthly temperature

Temperature is one of the important outputs from the WRF. The correlation coefficients between the WRF temperature and observations ranged from 0.91 to 0.99, averaged at 0.96, indicating that the WRF reasonably reproduced the spatial and temporal pattern of temperature (Figure 2a). Significant negative bias in temperature (Figure 2b) was found in the

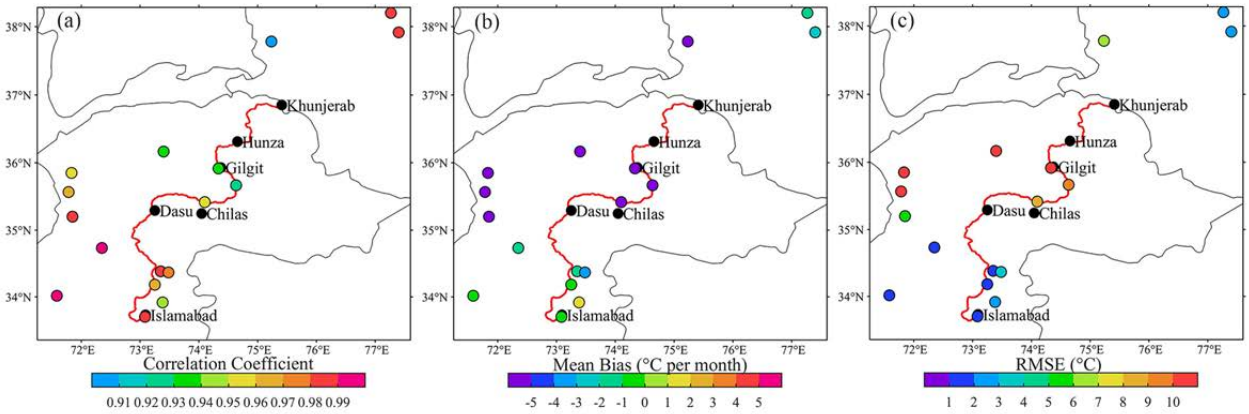

Figure 2 Mean monthly temperature correlation coefficients (a), mean bias (MB) (b), and Root Mean Square Error (RMSE) (c) of the Weather Research and Forecasting (WRF) model and in-situ observations.

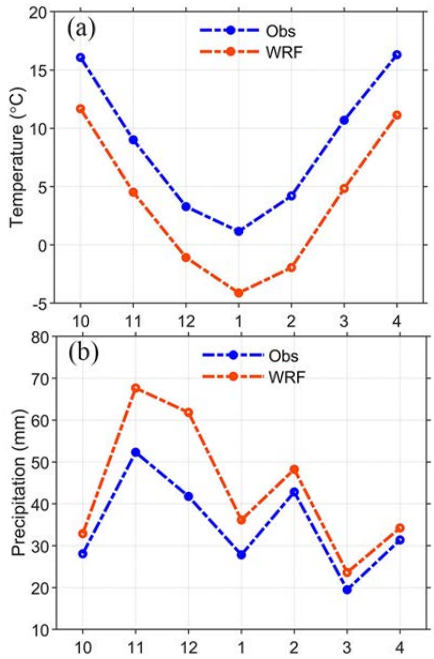

Figure 3 Mean monthly temperature (a) and precipitation (b) averaged from all stations of Weather Research and Forecasting (WRF) model and in-situ observation (Obs).

Karakoram and Central Himalaya regions in a former study (Norris et al. 2019). The RMSE of the WRF temperature varied by regions, with the highest error occurring mainly in the middle part of the study area (Figure 2c). Our results showed a negative bias of each month of less than 5°C in almost all stations with an average at -3.92°C (Figure 3a). The air temperature bias can be ascribed to various causes. One main cause is the difference in altitude between the model's grid and the in-situ stations due to the smoothed model terrain. This smooth topographic relief in the model could weaken the radiative fluxes and local circulation (Liu et al. 2019). According to a former study, the bias in temperature can be largely removed after the temperature lapse correction (Gao et al. 2015). In addition, the land surface type regulates the radiative and energy balance between the atmosphere and land. The air temperature and specific humidity are sensitive to the land surface type (He et al. 2017; Jiménez-Esteve et al. 2018). The mismatch in land use between the model and the real one in the in-situ stations could trigger a bias in the air temperature. Furthermore, systematic errors existed in the simulated wind speed from the WRF model (Heikkila et al. 2011), leading the bias in the simulated temperature advection.

Evaluating spatiotemporal distribution of temperature in study area is necessary, because high temperature is a trigger factor of wet snow avalanche activity in winter and early spring (Ballesteros-Cánovas et al. 2018). The main factor that influences the change in air temperature is the difference in terrain (He et al. 2017). The mean daily temperature of the WRF model during the cold season is shown in Figure 4a-h. The high temperature was noticed in the northeastern and southwestern part of the study area, as well as in the valley along the KKH, while the low temperature occurred in the high-elevation regions. The mean temperature measured below -25°C during the entire cold season at high elevations. The temperature seasonality was well reproduced by the WRF. The areas with < 0°C were extended from October, the coldest month was January with nearly < 0°C in the entire study area. Then, the

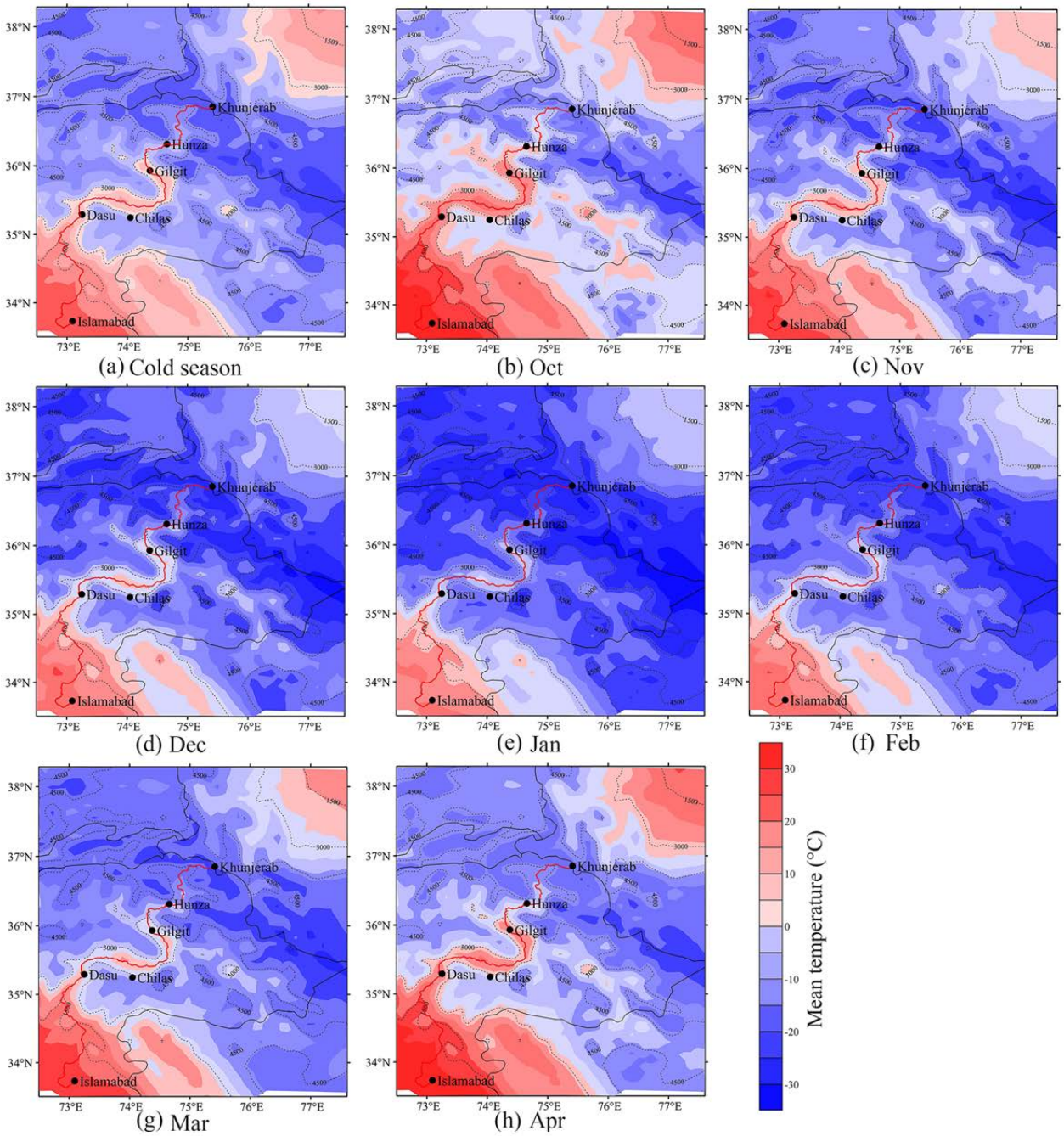

Figure 4 Spatial distribution of the mean temperature of the Weather Research and Forecasting (WRF) model during the entire cold season (a) and each month (b-h) during 2010-2015. The dashed line represents the elevation contours at 1500, 3000 and 4500 m.

temperature rose from March, but the low temperature was still seen at the high elevations.

2.2 Spatial and temporal patterns of the monthly precipitation

The month-by-month MB and RMSE were investigated between the WRF precipitation and observations (Figure 3b and Figure 5). The comparisons between the WRF and observations varied highly from station to station, with an average MB at 8.69 mm in all stations, but one to three times' overestimation in 11 stations (Figure 3b). The overestimation might be caused by the gauge measurements' systematic errors (Yang et al. 1999) and the model's structure and parameters

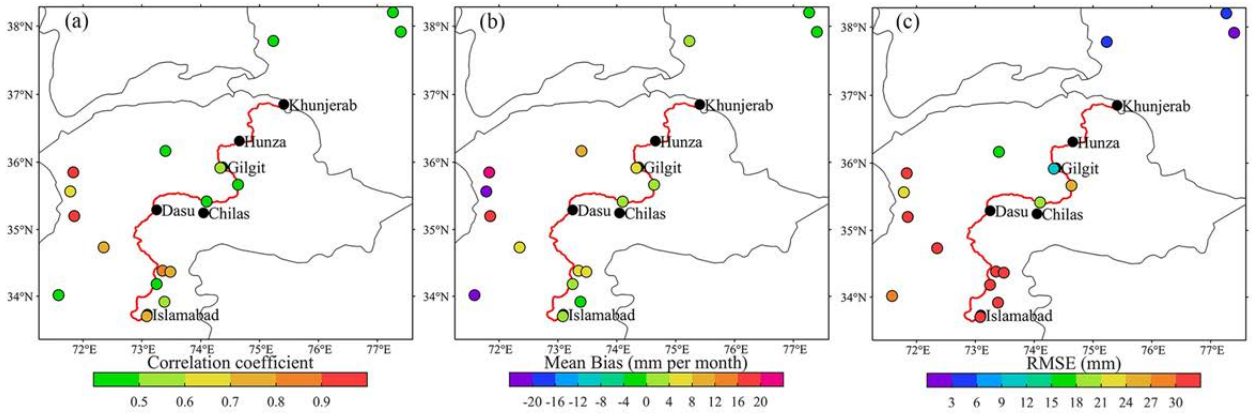

Figure 5 Mean monthly precipitation correlation coefficients (a), mean bias (MB) (b), and Root Mean Square Error (RMSE) (c) of the Weather Research and Forecasting (WRF) model and in-situ observations.

(Wang et al. 2018). The gauge-measured precipitation in the cold season exhibits a low undercatch due to the wind (Ye et al. 2004). In addition, the accuracy of forcing data and physical options could aggravate the overestimation of precipitation in the alpine regions (Pieri et al. 2015; Huang and Gao 2018). The precipitation data used in this study were measured by the tipping bucket. This kind of equipment measures the snowfall until it melts, and could not efficiently record the amount of snowfall if it was blown out of the gauge (Bollasina et al. 2002). This issue would bring a great undercatch of 20%-30% snowfall during winter in the highest elevation stations in Pakistan (Tahir et al. 2011). In addition, it was clear that large errors happened in the stations where the precipitation amount was high. For instance, the MB and RMSE were larger in the southwestern parts of the study area (Figure 5b and 5c), where the westerlies is dominated in the winter (Ahmad et al. 2018; Ullah et al. 2018). A sensitivity study proved that the response in precipitation amount to the temperature perturbations was larger at high elevations than that in low areas (Sandvik et al. 2018). This increased precipitation amount due to the bias in temperature, which was mainly caused by the mismatch in the elevation from the model and in-situ observations. The correlation coefficient (Figure 5a) between the monthly WRF precipitation and in-situ observations varied from 0.39 to 0.95, with an average at 0.57. This correlation was also revealed by the winter precipitation amount and extremes at low elevations in Pakistan (< 3000 m), although the total WRF precipitation amount was nearly three times larger than that of the in-situ observations (Collier and Immerzeel 2015; Norris et al. 2017). Additionally, no clear relationship between the elevation and precipitation was found. These results showed a large heterogeneity in the spatial patterns of precipitation arising from the complex terrain.

Figure 6 shows the five-year averaged precipitation amount from the WRF simulation in each month and the cold season, and the snow versus precipitation (S/P) ratio during the cold season over the entire study area. There existed two main high-value rain bands during the cold season according to Figure 6 a-h. They are located as a northwest-to-southeast direction around the KKH. The upper one was due to the high altitude, while the lower one was located in the windward slope of the westerlies. Additionally, it indicated that the precipitation mainly occurred in February and March. The monthly precipitation along the KKH mainly ranged from 1 to 30 mm from October to January but varied from 5 to 70 mm from February to April. The monthly precipitation revealed that the maximum precipitation over the entire simulating area was less than 80 mm in the period from October to January, while exceeded the 100 mm from February to April. The S/P ratio indicated that precipitation in the study area mainly occurred as the solid precipitation during the cold season except for the southern part and a small band between the Gilgit-Islamabad section (Figure 6i), which was consistent with the observations in the high altitude regions of the Tianshan Mountains, Switzerland and western United States (Serquet et al. 2011; Guo and Li 2015;

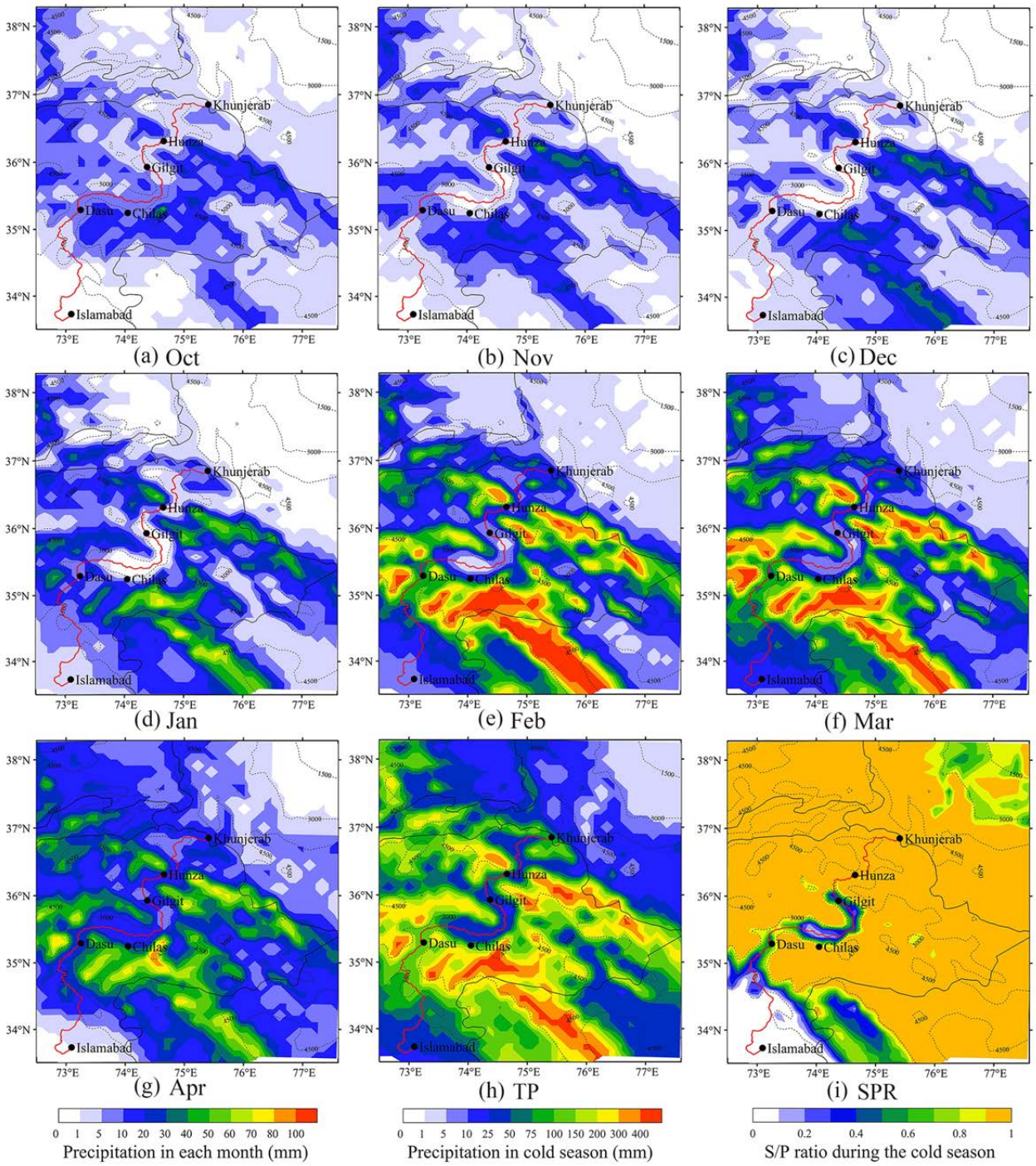

Figure 6 Spatial distribution of monthly precipitation (a-g), total precipitation (TP, h), and S/P ratio (SPR) (i) during the cold season from 2010 to 2015. The dashed line represents the elevation contours at 1500, 3000, and 4500 m.

Safeeq et al. 2016).

2.3 Daily and extreme precipitation during the cold season

It is important to assess the model capability to simulate precipitation frequency and intensity during the cold season, because they are directly linked to the snow hazards. Previous studies showed that most natural snow avalanches were triggered by heavy precipitation events and the accumulated amount of precipitation within a short period during the cold season (Hirashima et al. 2008; Gauthier et al. 2017; Hao et al. 2018). This

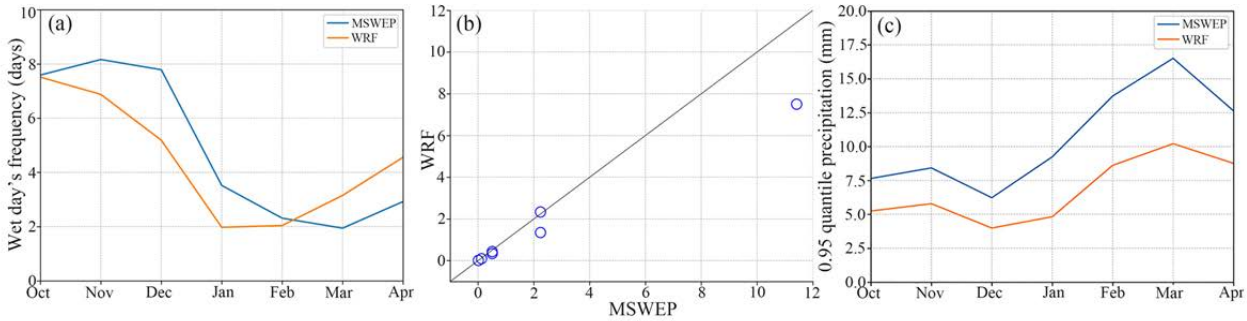

Figure 7 Wet days' frequency (> 1 mm, days) (a), different quantiles (0.1, 0.25, 0.5, 0.6, 0.7, 0.8 and 0.9 quantiles) (b), and extreme precipitation (0.95 quantile, mm) (c) of the total daily precipitation (mm day^{-1}) for the Weather Research and Forecasting (WRF) and Multi-Source Weighted-Ensemble Precipitation (MSWEP).

study compared the wet day frequency and intensity on a daily scale from the WRF precipitation and MSWEP datasets. The wet day frequency (> 1 mm) was shown in Figure 7a. Both the WRF and MSWEP precipitation exhibited more wet days in October, November, and December compared with the other months. The precipitation events were low in January and February from the WRF and also low in March from the MSWEP. The MSWEP precipitation demonstrated more wet days than the WRF precipitation did from October to February, while less during March and April (Figure 8). A high frequency of wet days in a northwest-to-southeast direction pattern was revealed by the WRF model (Figure 8a-g). The wet days were exceeding 25 days in January, February and March in the section between Hunza and Khunjerab. The high wet day frequency from the MSWEP precipitation has a northwest-to-southeast direction distribution (Figure 9h-n). However, the band of high wet frequency in the MSWEP precipitation did not extend to the centre of the study area. This was mainly due to the lack of gauges in the northwestern part of the study area, as the MSWEP dataset was generated in a gauge-based manner (Beck et al. 2019), leading to more uncertainties in precipitation in this area. It is also the strength that the WRF simulates over the ungauge area. In addition, the wet frequency from the WRF precipitation was smaller than that from the MSWEP precipitation.

The quantiles of the daily total precipitation during the entire cold season were shown in Figure 7b. The difference in the 0.1 to 0.6 quantiles between the WRF and MSWEP was small, indicating that the WRF model reproduced the quantiles well from 0.1 to 0.6. However, the WRF performed an underestimation on the 0.9 quantile. According to previous studies, the reanalysis data tend to overestimate the wet day frequency and to underestimate the intensity (Zolina et al. 2004; Sun et al. 2006; Stephens et al. 2010; Skok et al. 2016). This feature would pass to the output when reanalysis is forced in reproducing the precipitation.

The heavy precipitation events are often connected with hazardous consequences, such as snow avalanches, landslides, floods and so on. The precipitation could vary largely due to the geographical diversity, thus a fixed threshold is not suitable for the entire study area. In order to identify the extreme daily precipitation, the 0.95 quantile was used according to previous studies (Heikkila et al. 2011; Norris et al. 2015). The 0.95 quantile precipitation was low in October, November and December but nevertheless high in February, March, and April (Figure 7c). The MSWEP precipitation revealed higher values at the 0.95 quantile than the WRF precipitation, which could ascribe to the forcing data used by the WRF model underestimating the intensity (Zolina et al. 2004; Sun et al. 2006; Stephens et al. 2010; Skok et al. 2016). Figure 9 showed that the distribution of area with extreme values for the two precipitation datasets. The 0.95 quantile was high in WRF precipitation in February, March, and April (Figure 9 a-g), while occurred in January, February, March, and April in MSWEP precipitation (Figure 9 h-n), respectively. The areas with extreme values in WRF precipitation were smaller than those from the MSWEP precipitation, and they were mainly located in the windward slope of the westerlies in the study area. Specifically, the high values in WRF precipitation were mainly seen in the western part, but that in the MSWEP dataset concentrated in the southwestern part. This might be caused by the

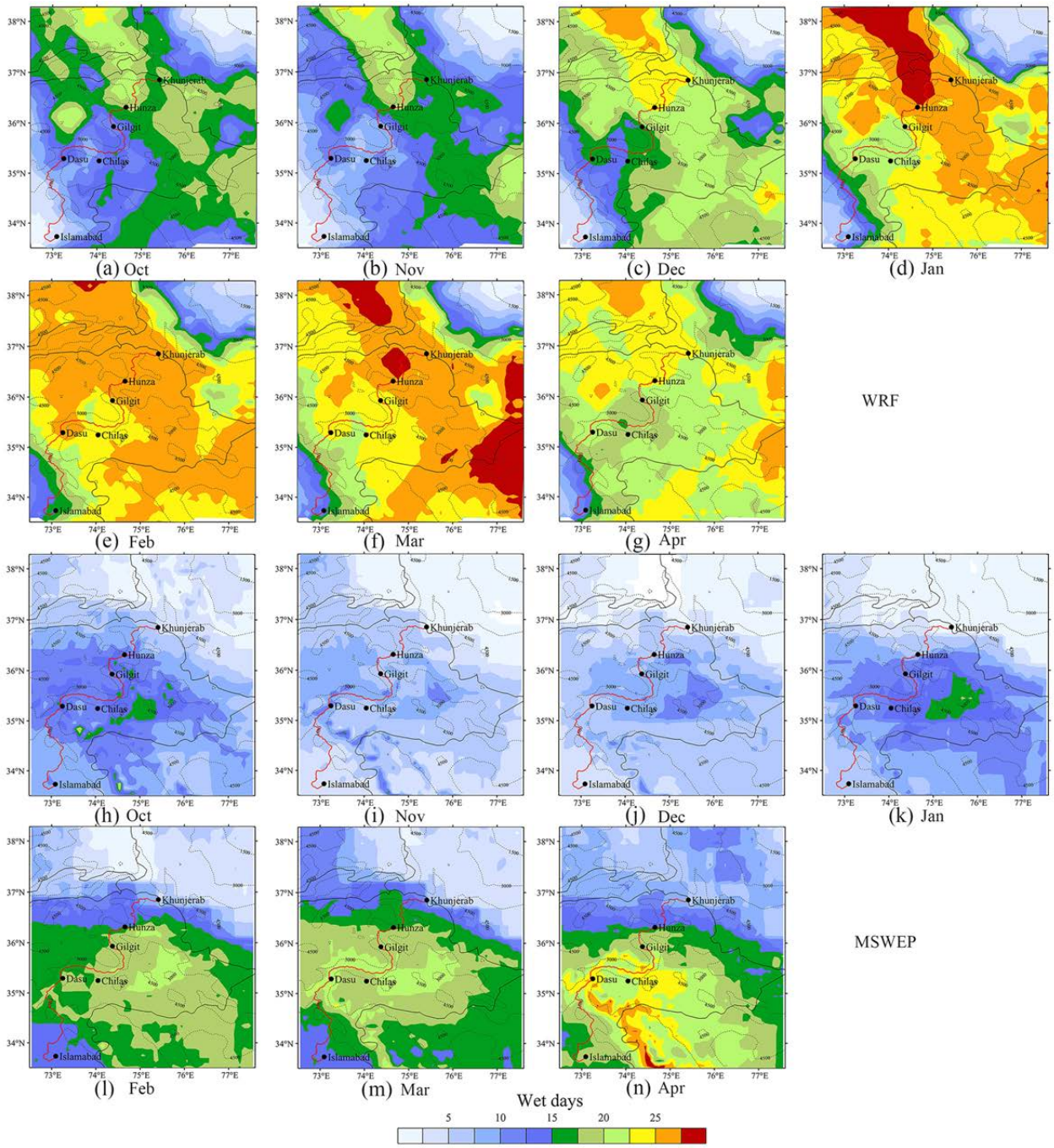

Figure 8 Spatial distribution of the Wet days' frequency (> 1 mm, days) in each month for the Weather Research and Forecasting (WRF) (a-g) and Multi-Source Weighted-Ensemble Precipitation (MSWEP) (h-n). The dashed line represents the elevation contours at 1500, 3000 and 4500 m.

rain gauges used in the MSWEP dataset, i.e. there exhibited an unbalanced distribution of rain gauges in the northwestern and southern part (Beck et al. 2019). Compared with the MSWEP precipitation, the distribution of extreme precipitation from the WRF revealed more terrain details. The areas with extreme values are located around almost each section of the KKH in February, March, and April, especially in the Dasu-Islamabad section. A sensitivity study indicated that the snowfall reduced in the steep slope but increased in the lower elevations in the topography smoothing experiment although the maximum precipitation magnitudes did not enhance in High Mountain

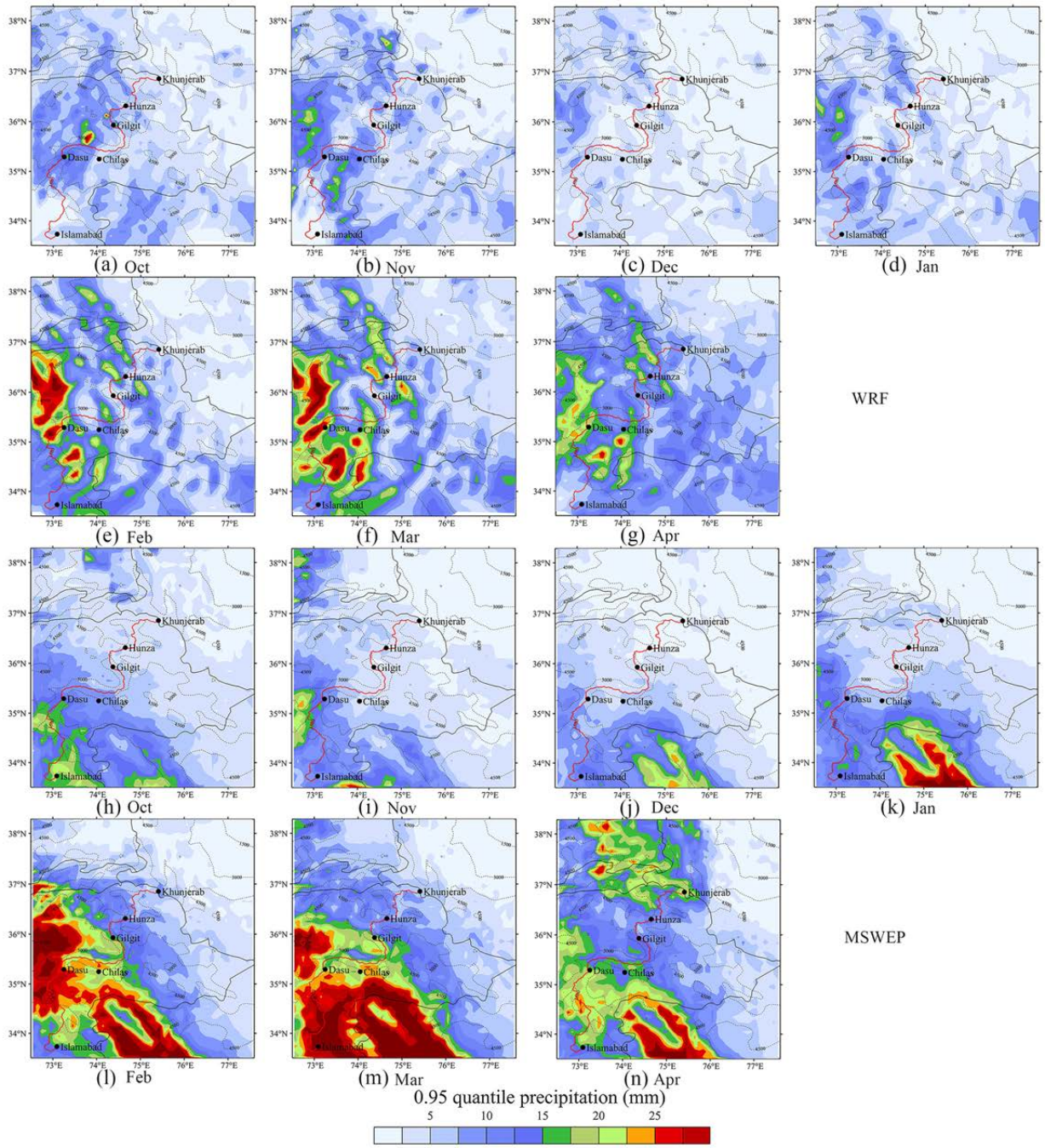

Figure 9 Spatial distribution of the daily extreme precipitation (0.95 quantile, mm) averaged in each month for the Weather Research and Forecasting (WRF) (a-g) and Multi-Source Weighted-Ensemble Precipitation (MSWEP) (h-n). The dashed line represents the elevation contours at 1500, 3000 and 4500 m.

Asia (Cannon et al. 2017). The heavy precipitation events during winter increased with the enhancement in strength and frequency of the winter westerlies in the Karakoram and western Himalaya area (Cannon et al. 2015). In addition, it is difficult to remove the mismatch between the grid dataset and in-situ observations. The dense observation network and multi-sources data assimilations could be used to correct the precipitation dataset, and potentially improve the accuracy of the grid dataset (Sun et al. 2018). Therefore, future work towards a simulation with the data assimilations at a finer resolution is necessary under the increasing westerlies' activity (Ridley et al. 2013).

3 Conclusion

The Karakoram with the complex topography and the large precipitation variability is a typically hazards-prone region. In this study, the regional climate model WRF simulation was performed at a 10 km grid over the Karakoram regions during the cold season from 2010 to 2015. The spatial and temporal patterns of temperature and precipitation were investigated with a special concern for the Karakoram Highway region, which helps to prevent snow related hazards during the cold season.

In order to evaluate the ability of the WRF, the in-situ observations of monthly mean temperature and precipitation have been used to compare with the WRF simulations, and the daily extreme precipitation patterns were evaluated by the MSWEP precipitation dataset. The WRF model exhibited a good capability to reproduce the observed monthly temperature (R = 0.96, mean bias = -3.92°C) and precipitation (R = 0.57, mean bias = 8.69 mm). Although the WRF model tended to overestimate the wet days frequency and to underestimate the intensity, it captured a realistic pattern of precipitation with high wet days frequency and extreme values. The high wet days frequency was seen in January, February and March in the region between Hunza and Khunjerab. In addition, the areas with extreme values were located in the high altitude areas around each section of the KKH in February, March, and April, especially the Dasu-Islamabad section. Considering the bias in precipitation and temperature, a sensitivity study of different forcing datasets, land cover types, parameterizations of cumulus scheme and microphysics scheme for study area should be performed to get the optimal parameterizations in the next work, which could help improving the downscaling performance of precipitation and temperature using the WRF model.

Acknowledgments

This work is financially supported by the project of the National Natural Science Foundation of China (U1703241), the Strategic Priority Research Program of the Chinese Academy of Sciences, the Pan-Third Pole Environment Study for a Green Silk Road (Pan-TPE) (XDA2004030202), the Chinese Academy of Sciences President's International Fellowship Initiative (PIFI, Grant No. 2017VCA0002) and the China Scholarship Council (CSC, Grant No. 201904910896).

References

Ahmad I, Zhang F, Tayyab M, et al. (2018) Spatiotemporal analysis of precipitation variability in annual, seasonal and extreme values over upper Indus River basin. Atmospheric Research 213: 346-360. https://doi.org/10.1016/j.atmosres.2018.06.019

Anders AM, Roe GH, Hallet B, et al. (2006) Spatial patterns of precipitation and topography in the Himalaya. In: Geological Society of America (Special Paper) 398: 39-53. https://doi.org/10.1130/2006.2398(03)

Antic S, Laprise R, Denis B, et al. (2006) Testing the downscaling ability of a one-way nested regional climate model in regions of complex topography. Climate Dynamics 26(2-3):305-325. https://doi.org/10.1007/s00382-004-0438-5

Argüeso D, Hidalgo-Muñoz JM, Gámiz-Fortis SR, et al. (2012) Evaluation of WRF mean and extreme precipitation over Spain: present climate (1970–99). Journal of Climate 25(14): 4883-4897. https://doi.org/10.1175/JCLI-D-11-00276.1

Ashraf A, Naz R, Roohi R (2012). Glacial lake outburst flood hazards in Hindukush, Karakoram and Himalayan Ranges of Pakistan: implications and risk analysis. Geomatics, Natural Hazards and Risk 3(2): 113-132. https://doi.org/10.1080/19475705.2011.615344

Asmat U, Athar H (2017) Run-based multi-model interannual variability assessment of precipitation and temperature over Pakistan using two IPCC AR4-based AOGCMs. Theoretical and Applied Climatology 127(1-2): 1-16. https://doi.org/10.1007/s00704-015-1616-6

Avolio E, Federico S (2018) WRF simulations for a heavy rainfall event in southern Italy: Verification and sensitivity tests. Atmospheric Research 209: 14-35. https://doi.org/10.1016/j.atmosres.2018.03.009

Ballesteros-Cánovas J A, Trappmann D, Madrigal-González J, et al. (2018) Climate warming enhances snow avalanche risk in the Western Himalayas. Proceedings of the National Academy of Sciences 115(13): 3410-3415. https://doi.org/10.1073/pnas.1716913115

Beck HE, Van Dijk AI, Levizzani V, et al. (2017) MSWEP: 3-hourly 0.25 global gridded precipitation (1979-2015) by merging gauge, satellite, and reanalysis data. Hydrology and Earth System Sciences 21(1): 589-615. https://doi.org/10.5194/hess-21-589-2017

Beck HE, Vergopolan N, Pan M, et al. (2020) Global-scale evaluation of 22 precipitation datasets using gauge observations and hydrological modeling. In: Satellite Precipitation Measurement. Springer, Cham. pp 625-653. https://doi.org/10.1007/978-3-030-35798-6_9

Beck HE, Wood EF, Pan M, et al. (2019) MSWEP V2 global 3-hourly 0.1 precipitation: methodology and quantitative assessment. Bulletin of the American Meteorological Society 100(3): 473-500. https://doi.org/10.1175/BAMS-D-17-0138.1

Bollasina M, Bertolani L, Tartari G (2002) Meteorological observations at high altitude in the Khumbu Valley, Nepal Himalayas, 1994-1999. Bulletin of Glaciological Research 19: 1-12.

Bolch T, Kulkarni A, Kääb A, et al. (2012) The state and fate of Himalayan glaciers. Science 336(6079): 310-314. https://doi.org/10.1126/science.1215828

Cannon F, Carvalho LM, Jones C, et al. (2015) Multi-annual variations in winter westerly disturbance activity affecting the Himalaya. Climate Dynamics 44(1-2): 441-455. https://doi.org/10.1007/s00382-014-2248-8

Cannon F, Carvalho LM, Jones C, et al. (2017) Effects of topographic smoothing on the simulation of winter precipitation in High Mountain Asia. Journal of Geophysical Research: Atmospheres 122(3): 1456-1474. https://doi.org/10.1002/2016JD026038

Cardoso RM, Soares PMM, Miranda PMA, et al. (2013) WRF

high resolution simulation of Iberian mean and extreme precipitation climate. International Journal of Climatology 33(11): 2591-2608. https://doi.org/10.1002/joc.3616
Chen F, Dudhia J (2001) Coupling an advanced land surface–hydrology model with the Penn State–NCAR MM5 modeling system. Part I: Model implementation and sensitivity. Monthly Weather Review 129(4): 569-585. https://doi.org/10.1175/1520-0493(2001)129<0569:CAALSH>2.0.CO;2.
Chen L, Dirmeyer PA (2017) Impacts of land-use/land-cover change on afternoon precipitation over North America. Journal of Climate 30(6): 2121-2140. https://doi.org/10.1175/JCLI-D-16-0589.1
Chen L, Dirmeyer PA, Tawfik A, et al. (2017) Sensitivities of land cover–precipitation feedback to convective triggering. Journal of Hydrometeorology 18(8): 2265-2283. https://doi.org/10.1175/jhm-d-17-0011.1
Collier E, Immerzeel WW (2015) High‐resolution modeling of atmospheric dynamics in the Nepalese Himalaya. Journal of Geophysical Research: Atmospheres 120(19): 9882-9896. https://doi.org/10.1002/2015JD023266.
Derbyshire E, Fort M, Owen LA (2001) Geomorphological Hazards along the Karakoram Highway: Khunjerab Pass to the Gilgit River, Northernmost Pakistan (Geomorphologische Hazards entlang des Karakorum Highway: Khunjerab Paß bis zum Gilgit River, nördlichstes Pakistan). Erdkunde 49-71. https://www.jstor.org/stable/25647347
Dimri AP, Niyogi D, Barros AP, et al. (2015) Western disturbances: a review. Reviews of Geophysics 53(2): 225-246. https://doi.org/10.1002/2014RG000460.
Dudhia J (1989) Numerical study of convection observed during the winter monsoon experiment using a mesoscale two-dimensional model. Journal of the Atmospheric Sciences 46(20): 3077-3107. https://doi.org/10.1175/1520-0469(1989)046<3077:NSOCOD>2.0.CO;2
El-Samra R, Bou-Zeid E, Bangalath HK, et al. (2017) Future intensification of hydro-meteorological extremes: downscaling using the weather research and forecasting model. Climate Dynamics 49(11-12): 3765-3785. https://doi.org/10.1007/s00382-017-3542-z
Erlandsen HB, Haddeland I, Tallaksen LM, et al. (2017) The sensitivity of the terrestrial surface energy and water balance estimates in the WRF model to lower surface boundary representations: A South Norway case study. Journal of Hydrometeorology 18(1): 265-284. https://doi.org/10.1175/JHM-D-15-0146.1
Fernández‐González S, Valero F, Sánchez JL, et al. (2015) Numerical simulations of snowfall events: Sensitivity analysis of physical parameterizations. Journal of Geophysical Research: Atmospheres 120(19): 10-130. https://doi:10.1002/2015JD023793.
Funk C, Peterson P, Landsfeld M, et al. (2015) The climate hazards infrared precipitation with stations—a new environmental record for monitoring extremes. Scientific Data 2(1): 1-21. https://doi.org/10.1038/sdata.2015.66
Gao Y, Xu J, Chen D (2015) Evaluation of WRF mesoscale climate simulations over the Tibetan Plateau during 1979–2011. Journal of Climate 28(7): 2823-2841. https://doi.org/10.1175/JCLI-D-14-00300.1
Gauthier F, Germain D, Hétu B (2017) Logistic models as a forecasting tool for snow avalanches in a cold maritime climate: northern Gaspésie, Québec, Canada. Natural Hazards 89(1): 201-232. https://doi.org/10.1007/s11069-017-2959-3
Gula J, Peltier WR (2012) Dynamical downscaling over the Great Lakes basin of North America using the WRF regional climate model: The impact of the Great Lakes system on regional greenhouse warming. Journal of Climate 25(21): 7723-7742. https://doi.org/10.1175/JCLI-D-11-00388.1
Guo L, Li L (2015). Variation of the proportion of precipitation occurring as snow in the Tian Shan Mountains, China. International Journal of Climatology 35(7): 1379-1393. https://doi.org/10.1002/joc.4063
Harris IPDJ, Jones PD, Osborn TJ, et al. (2014) Updated high‐resolution grids of monthly climatic observations–the CRU TS3. 10 Dataset. International Journal of Climatology 34(3): 623-642. https://doi.org/10.1002/joc.3711
Hao JS, Huang FR, Liu Y, et al. (2018) Avalanche activity and characteristics of its triggering factors in the western Tianshan Mountains, China. Journal of Mountain Science 15(7): 1397-1411. https://doi.org/10.1007/s11629-018-4941-2
Hasson S, Lucarini V, Khan MR, et al. (2014) Early 21st century snow cover state over the western river basins of the Indus River system. Hydrology and Earth System Sciences 18: 4077-4100. https://doi.org/10.5194/hess-18-4077-2014
He JJ, Yu Y, Yu LJ, et al. (2017) Impacts of uncertainty in land surface information on simulated surface temperature and precipitation over China. International Journal of Climatology 37: 829-847. https://doi.org/10.1002/joc.5041
Heikkilä U, Sandvik A, Sorteberg A (2011) Dynamical downscaling of ERA-40 in complex terrain using the WRF regional climate model. Climate Dynamics 37(7-8): 1551-1564. https://doi.org/10.1007/s00382-010-0928-6
Hirashima H, Nishimura K, Yamaguchi S, et al. (2008) Avalanche forecasting in a heavy snowfall area using the snowpack model. Cold Regions Science and Technology 51(2-3): 191-203. https://doi.org/10.1016/j.coldregions.2007.05.013
Hong SY, Lim JOJ (2006) The WRF single-moment 6-class microphysics scheme (WSM6). Asia-Pacific Journal of Atmospheric Sciences 42(2): 129-151.
Houze Jr RA, Rasmussen KL, Medina S, et al. (2011) Anomalous atmospheric events leading to the summer 2010 floods in Pakistan. Bulletin of the American Meteorological Society 92(3): 291-298. https://doi.org/10.1175/2010BAMS3173.1
Huang D, Gao S (2018) Impact of different reanalysis data on WRF dynamical downscaling over China. Atmospheric Research 200: 25-35. https://doi.org/10.1016/j.atmosres.2017.09.017
Huffman GJ, Bolvin DT, Nelkin EJ, et al. (2007) The TRMM multisatellite precipitation analysis (TMPA): Quasi-global, multiyear, combined-sensor precipitation estimates at fine scales. Journal of Hydrometeorology 8(1): 38-55. https://doi.org/10.1175/JHM560.1
Ikeda K, Rasmussen R, Liu C, et al. (2010) Simulation of seasonal snowfall over Colorado. Atmospheric Research 97(4): 462-477.https://doi.org/10.1016/j.atmosres.2010.04.010
Jiménez-Esteve B, Udina M, Soler MR, et al. (2018) Land use and topography influence in a complex terrain area: A high resolution mesoscale modelling study over the Eastern Pyrenees using the WRF model. Atmospheric Research 202: 49-62. https://doi.org/10.1016/j.atmosres.2017.11.012
Kain JS (2004) The Kain–Fritsch convective parameterization: an update. Journal of Applied Meteorology 43(1): 170-181. https://doi.org/10.1175/1520-0450(2004)043<0170:TKCPAU>2.0.CO;2
Karki R, ul Hasson S, Gerlitz L, et al. (2018) WRF-based simulation of an extreme precipitation event over the Central Himalayas: Atmospheric mechanisms and their representation by microphysics parameterization schemes. Atmospheric Research 214: 21-35. https://doi.org/10.1016/j.atmosres.2018.07.016
Koks EE, Rozenberg J, Zorn C, et al. (2019) A global multi-hazard risk analysis of road and railway infrastructure assets. Nature Communications 10(1): 1-11. https://doi.org/10.1038/s41467-019-10442-3
Kreutzmann H (2004) Accessibility for High Asia: Comparative perspectives on northern Pakistan's traffic infrastructure and linkages with its neighbours in the Hindukush-Karakoram-Himalaya. Journal of Mountain Science 1(3): 193-210. https://link.springer.com/article/10.1007/BF02919325
Lang TJ, Barros AP (2004) Winter storms in the central Himalayas. Journal of the Meteorological Society of Japan. Ser. II 82(3): 829-844.https://doi.org/10.2151/jmsj.2004.829
Lettenmaier DP, Alsdorf D, Dozier J, et al. (2015) Inroads of remote sensing into hydrologic science during the WRR era. Water Resources Research 51(9): 7309-7342. https://doi.org/10.1111/j.1752-1688.1969.tb04897.x
Li Q, Yang T, Qi Z, et al. (2018) Spatiotemporal variation of snowfall to precipitation ratio and its implication on water resources by a regional climate model over Xinjiang, China. Water 10(10): 1463. https://doi.org/10.3390/w10101463
Liu C, Ikeda K, Rasmussen R, et al. (2017) Continental-scale convection-permitting modeling of the current and future climate of North America. Climate Dynamics 49(1-2): 71-95. https://doi.org/10.1007/s00382-016-3327-9
Liu L, Ma Y, Menenti M, et al. (2019) Evaluation of WRF modeling in relation to different land surface schemes and initial and boundary conditions: A snow event simulation over the Tibetan Plateau. Journal of Geophysical Research: Atmospheres 124(1): 209-226. https://doi.org/10.1029/2018JD029208

Maussion F, Scherer D, Finkelnburg R, et al. (2011) WRF simulation of a precipitation event over the Tibetan Plateau, China--an assessment using remote sensing and ground observations. Hydrology and Earth System Sciences 15(6). https://doi.org/10.5194/hess-15-1795-2011
Maussion F, Scherer D, Mölg T, et al. (2014) Precipitation seasonality and variability over the Tibetan Plateau as resolved by the High Asia Reanalysis. Journal of Climate 27(5): 1910-1927. https://doi.org/10.1175/JCLI-D-13-00282.1
Mlawer EJ, Taubman SJ, Brown PD, et al. (1997) Radiative transfer for inhomogeneous atmospheres: RRTM, a validated correlated‐k model for the longwave. Journal of Geophysical Research: Atmospheres 102(D14): 16663-16682. https://doi.org/10.1029/97JD00237
Norris J, Carvalho LM, Jones C, et al. (2019) Deciphering the contrasting climatic trends between the central Himalaya and Karakoram with 36 years of WRF simulations. Climate Dynamics 52(1-2): 159-180. https://doi.org/10.1007/s00382-018-4133-3
Norris J, Carvalho LM, Jones C, et al. (2015) WRF simulations of two extreme snowfall events associated with contrasting extratropical cyclones over the western and central Himalaya. Journal of Geophysical Research: Atmospheres 120(8): 3114-3138. https://doi.org/10.1002/2014JD022592
Norris J, Carvalho LM, Jones C, et al. (2017) The spatiotemporal variability of precipitation over the Himalaya: evaluation of one-year WRF model simulation. Climate Dynamics 49(5-6): 2179-2204. https://doi.org/10.1007/s00382-016-3414-y
Pieri AB, von Hardenberg J, Parodi A, et al. (2015) Sensitivity of precipitation statistics to resolution, microphysics, and convective parameterization: A case study with the high-resolution WRF climate model over Europe. Journal of Hydrometeorology 16(4): 1857-1872. https://doi.org/10.1175/JHM-D-14-0221.1
Prakash S (2019) Performance assessment of CHIRPS, MSWEP, SM2RAIN-CCI, and TMPA precipitation products across India. Journal of Hydrology 571: 50-59. https://doi.org/10.1016/j.jhydrol.2019.01.036
Qiu Y, Hu Q, Zhang C (2017) WRF simulation and downscaling of local climate in Central Asia. International Journal of Climatology 37: 513-528. https://doi.org/10.1002/joc.5018
Rasmussen R, Baker B, Kochendorfer J, et al. (2012) How well are we measuring snow: The NOAA/FAA/NCAR winter precipitation test bed. Bulletin of the American Meteorological Society 93(6): 811-829. https://doi.org/10.1175/BAMS-D-11-00052.1
Ridley J, Wiltshire A, Mathison C (2013) More frequent occurrence of westerly disturbances in Karakoram up to 2100. Science of the Total Environment 468: S31-S35. https://doi.org/10.1016/j.scitotenv.2013.03.074
Safeeq M, Shukla S, Arismendi I, et al. (2016) Influence of winter season climate variability on snow–precipitation ratio in the western United States. International Journal of Climatology 36(9): 3175-3190. https://doi.org/10.1002/joc.4545
Sandvik MI, Sorteberg A, Rasmussen R (2018) Sensitivity of historical orographically enhanced extreme precipitation events to idealized temperature perturbations. Climate dynamics 50(1-2): 143-157. https://doi.org/10.1007/s00382-017-3593-1
Schellekens J, Dutra E, la Torre AMD, et al. (2017) A global water resources ensemble of hydrological models: The eartH2Observe Tier-1 dataset. Earth System Science Data 9: 389-413. https://doi.org/10.5194/essd-9-389-2017
Schneider U, Becker A, Finger P, et al. (2014) GPCC's new land surface precipitation climatology based on quality-controlled in situ data and its role in quantifying the global water cycle. Theoretical and Applied Climatology 115(1-2): 15-40. https://doi.org/10.1007/s00704-013-0860-x
Serquet G, Marty C, Dulex JP, et al. (2011) Seasonal trends and temperature dependence of the snowfall/precipitation‐day ratio in Switzerland. Geophysical research letters 38(7). https://doi.org/10.1029/2011GL046976
Skamarock WC, Klemp JB, Dudhia J, et al. (2005) A description of the advanced research WRF version 2 (No. NCAR/TN-468+ STR). National Center For Atmospheric Research Boulder Co Mesoscale and Microscale Meteorology Div. http://www. mmm. ucar. edu/wrf/users/docs/arw_v2. pdf.
Skamarock WC, Klemp JB (2008) A time-split nonhydrostatic atmospheric model for weather research and forecasting applications. Journal of Computational Physics 227(7): 3465-3485.https://doi.org/10.1016/j.jcp.2007.01.037
Skok G, Žagar N, Honzak L, et al. (2016) Precipitation intercomparison of a set of satellite-and raingauge-derived datasets, ERA Interim reanalysis, and a single WRF regional climate simulation over Europe and the North Atlantic. Theoretical and Applied Climatology 123(1-2): 217-232. https://doi.org/10.1007/s00704-014-1350-5
Stephens GL, L'Ecuyer T, Forbes R, et al. (2010) Dreary state of precipitation in global models. Journal of Geophysical Research: Atmospheres 115(D24). https://doi.org/10.1029/2010JD014532
Sun Q, Miao C, Duan Q, et al. (2018) A review of global precipitation data sets: Data sources, estimation, and intercomparisons. Reviews of Geophysics 56(1): 79-107. https://doi.org/10.1002/2017RG000574
Sun Y, Solomon S, Dai A, et al. (2006) How often does it rain?. Journal of Climate 19(6): 916-934. https://doi.org/10.1175/JCLI3672.1
Tahir AA, Chevallier P, Arnaud Y, et al. (2011) Snow cover dynamics and hydrological regime of the Hunza River basin, Karakoram Range, Northern Pakistan. Hydrology and Earth System Sciences 15 (7): 2275-2290. https://doi.org/10.5194/hess-15-2275-2011
Tang J, Niu X, Wang S, et al. (2016) Statistical downscaling and dynamical downscaling of regional climate in China: Present climate evaluations and future climate projections. Journal of Geophysical Research: Atmospheres 121(5): 2110-2129. https://doi.org/10.1002/2015JD023977
Ullah S, You Q, Ullah W, et al. (2018) Observed changes in precipitation in China-Pakistan economic corridor during 1980–2016. Atmospheric Research 210: 1-14. https://doi.org/10.1016/j.atmosres.2018.04.007
Ullah W, Wang G, Ali G, et al. (2019) Comparing multiple precipitation products against in-situ observations over different climate regions of Pakistan. Remote Sensing 11(6): 628. https://doi.org/10.3390/rs11060628
Wang X, Pang G, Yang M (2018) Precipitation over the Tibetan Plateau during recent decades: a review based on observations and simulations. International Journal of Climatology 38(3): 1116-1131. https://doi.org/10.1002/joc.5246
Wang Y, Geerts B, Liu C (2018) A 30‐year convection‐permitting regional climate simulation over the interior western United States. Part I: Validation. International Journal of Climatology 38(9): 3684-3704. https://doi.org/10.1002/joc.5527
Xie P, Xiong AY (2011) A conceptual model for constructing high‐resolution gauge‐satellite merged precipitation analyses. Journal of Geophysical Research: Atmospheres 116(D21). https://doi.org/10.1029/2011JD016118
Xu Z, Wu Z, He H, et al. (2019) Evaluating the accuracy of MSWEP V2. 1 and its performance for drought monitoring over mainland China. Atmospheric Research 226: 17-31. https://doi.org/10.1016/j.atmosres.2019.04.008
Yang D, Ishida S, Goodison BE, et al. (1999) Bias correction of daily precipitation measurements for Greenland. Journal of Geophysical Research: Atmospheres 104(D6): 6171-6181. https://doi.org/10.1029/1998JD200110
Yang T, Li Q, Chen X, et al. (2020) Spatiotemporal variability of the precipitation concentration and diversity in Central Asia. Atmospheric Research 104954. https://doi.org/10.1016/j.atmosres.2020.104954
Yatagai A, Kamiguchi K, Arakawa O, et al. (2012) APHRODITE: Constructing a long-term daily gridded precipitation dataset for Asia based on a dense network of rain gauges. Bulletin of the American Meteorological Society 93(9): 1401-1415. https://doi.org/10.1175/BAMS-D-11-00122.1
Ye B, Yang D, Ding Y, et al. (2004) A bias-corrected precipitation climatology for China. Journal of Hydrometeorology 5(6): 1147-1160. https://doi.org/10.1175/JHM-366.1
Yuan X, Liang XZ, Wood EF (2012) WRF ensemble downscaling seasonal forecasts of China winter precipitation during 1982–2008. Climate Dynamics 39(7-8): 2041-2058. https://doi.org/10.1007/s00382-011-1241-8
Zolina O, Kapala A, Simmer C, et al. (2004) Analysis of extreme precipitation over Europe from different reanalyses: a comparative assessment. Global and Planetary Change 44(1-4): 129-161. https://doi.org/10.1016/j.gloplacha.2004.06.009